Solid State Sciences 11 (2009) 1088–1093

Contents lists available at ScienceDirect

Solid State Sciences

journal homepage: www.elsevier.com/locate/ssscie

Controllable growth of silver nanostructures by a simple replacement reaction and their SERS studies

Weichun Ye [a,b], Chengmin Shen [b], Jifa Tian [b], Chunming Wang [a,*], Chao Hui [b], Hongjun Gao [b,*]

[a] Department of Chemistry, Lanzhou University, Tianshui Road No. 298, Lanzhou 730000, China
[b] Beijing National Laboratory for Condensed Matter Physics, Institute of Physics, Chinese Academy of Sciences, Beijing 100080, China

ARTICLE INFO

Article history:
Received 4 September 2008
Received in revised form
6 January 2009
Accepted 2 March 2009
Available online 10 March 2009

Keywords:
Structural evolution
Replacement reaction
Surface-enhanced Raman scattering (SERS)
Open circuit potential-time (Ocp-t)

ABSTRACT

Hierarchical silver nanostructures, consisting of dendritic (symmetric branched) and fractal patterns (randomly ramified), were synthesized very easily by dropping a droplet of $AgNO_3$-HF solution on silicon wafers. Scanning electron microscopy (SEM), X-ray diffraction (XRD) and open circuit potential-time (Ocp-t) measurement demonstrated that the two nanostructures converted with the reaction composition. The structural evolution was tentatively explained with the theory that oriented growth was determined by the anisotropy of the solid–liquid interfacial energy and the oriented attachment-based aggregation mechanism. Results on surface-enhanced Raman scattering (SERS) signals of the silver films with hierarchical nanostructures demonstrate that SERS is sensitive to silver nanostructures.

1. Introduction

In general, hierarchical nanostructures of noble metal consist of dendritic (symmetric branched) and fractal patterns (randomly ramified). They are two structural forms generated under non-equilibrium conditions and have promising applications in novel electronic systems, catalysis, sensing, and surface-enhanced Raman scattering (SERS) [1–4]. It is believed that the diffusion-limited aggregation (DLA) effect and anisotropic crystal growth play an identically important role in the formation of dendrites [5–8], and hence the morphological diversity of the resulting dendritic structures can be achieved and tuned by balancing the two factors.

Up to date, there have been many theoretical attempts to disclose the structural evolution in dendritic growth [9–15]. For example, Haxhimali et al. [9] believed that orientation selection was primarily determined by the anisotropy of the solid–liquid interfacial energy, $\gamma(\tilde{n})$. An oriented attachment mechanism was developed to interpret the diversity of hierarchical dendritic silver nanostructures [10]. Fang et al. [11,12] suggested that the transition from fractal pattern to dendrite in silver was driven by the competition between the thermodynamic and kinetic factors. Nevertheless, the fundamental issues on controlling the fractal and dendritic growth are still not clear.

Since the first observation of SERS by Fleischmann et al. in 1974 [16], this technology has emerged as a routine and powerful tool for structural characterization of interfaces and molecularly thin-films, due to the high surface sensitivity and selectivity. SERS occurring on roughened metal substrates, such as silver, gold and copper, in principle provides a powerful means of obtaining vibration information on adsorbate–surface interactions, taking advantage of high sensitivity and excellent frequency resolution. Although the detailed mechanism of SERS enhancement has not been fully understood, SERS is generally explained by two different kinds of mechanisms [17]: one is attributed to the local electromagnetic field at the metal surface or rough metal structures due to the surface plasmon polaritons, while the other is a chemical contribution due to an electronic resonance energy transfer between absorbed molecules and the metal surface. Therefore, control over the composition, shape, size, and local environment of surface structure is vital to achieve consistent SERS enhancement.

A replacement reaction is a simple approach to synthesize in a number of nanostructured materials [18–20]. The silver-engaged replacement reaction can, in principle, be extended to the reduction by any anodic process whose redox potential is lower than that of Ag^+/Ag pair. Here, we have developed a simple approach to synthesize silver nanodendrites, in which a droplet of aqueous solution of HF-$AgNO_3$ was dipped onto a silicon surface at room temperature and the silver structure evolution from nanoparticles (or nanoclusters) to dendrites, and to fractal structures proceeded gradually. Distinctive SERS features on silver nanostructures at

* Corresponding authors. Tel.: +86 931 8911895; fax: +86 931 8912582.
E-mail addresses: wangcm@lzu.edu.cn (C. Wang), hjgao@aphy.iphy.ac.cn (H. Gao).

1293-2558/$ – see front matter © 2009 Elsevier Masson SAS. All rights reserved.
doi:10.1016/j.solidstatesciences.2009.03.001

different stages were obtained using Rhodamine 6G (R6G) as probing molecule.

2. Experimental

2.1. Growth of Ag nanostructures

The p-type silicon (111) wafers were cleaned with acetone and ethanol to remove possible contaminants, and then etched in a 5 wt% HF solution for 10 min to prepare a clean, hydrogen-terminated surface. The wafers were rinsed with water and dried with dry nitrogen flux after each cleaning step. Droplets (30 μL) of a 1.0 M HF solution containing 0.1 M silver nitrate (Acros) were delivered to the hydrogen-terminated surfaces to react for 10 s (Sample 1), 30 s (Sample 2), 1 min (Sample 3) and 5 min (Sample 4) at room temperature in ambient environment. The samples were rinsed with water and dried in air. All reagents were used without further treatment. Double distilled water was used through out the experiments.

As for Sample 5, the fabrication process was performed as follows: the first droplet of 1.0 M HF solution containing 0.1 M silver nitrate was etched the wafer for 5 min, and rinsed with water, and then another droplet (30 μL) of 1.0 M HF solution containing 0.1 M silver nitrate reacted for 1 min.

As for Sample 6, using 1.0 M NH_4F containing 0.1 M silver nitrate to replace $AgNO_3$-HF solution, 30 μL was dropleted to the hydrogen-terminated surfaces to react for 5 min.

2.2. Characterization of Ag nanostructures

The morphologies of the samples were observed by a field-emission scanning electron microscope (FE-SEM; Model XL-SFEG; FEI Corp.). The X-ray diffraction (XRD) patterns were recorded using an X-ray diffraction analyzer (XRD, Rigaku D/max-2400, Cu Kα radiation, $\lambda = 0.1541$ nm).

2.3. Ocp-t measurement

Open circuit potential-time (Ocp-t) measurement was carried out with a CHI-614A electrochemical workstation (made in Shanghai, China). The etched silicon wafer served as the working electrode. The counter electrode was a platinum wire, and the reference one was an Ag/AgCl wire. The electrolyte was 150 μL of 1.0 M HF + 0.1 M $AgNO_3$ solution. As the electrolyte was added, the scanning started immediately, so the information of the reaction was recorded from 0 s.

2.4. SERS measurements

Samples used for SERS evaluations were prepared by dipping Sample 2, Sample 4 and Sample 6 in 10 μM and 1 nM R6G ethanol solution for 30 min, respectively. The samples were then taken out, rinsed using ethanol for three times, and dried in air. The Raman scattering measurements were performed at room temperature on a Raman system (JY-HR800) with confocal microscopy. The solid-state diode laser (533 nm) was used as an excitation source. The laser power on the samples was kept with 1 mW and the typical spectrum acquisition time was 30 s. The probed area was about 1 μm in diameter with a 50× microscope objective lens.

3. Results and discussion

3.1. Morphological evolution

The synthetic process of Ag nanostructures is illustrated in Fig. 1. As 30 μL of 1.0 M HF solution containing 0.1 M $AgNO_3$ was dropped onto silicon surface. Fast etching of silicon by HF solution resulted in H-terminated surface that is intrinsically hydrophobic, so solution droplet exhibited semi-spherical shape. The concurrently occurred chemical reaction can be expressed as the following that led to generation of Ag:

$$4Ag^+ + Si(s) + 6F^- \rightarrow 4Ag(s) + SiF_6^{2-} \quad (1)$$

which can be divided into two half-cell reactions (2) and (3)

$$\text{Cathodic } Ag^+ + e^- \rightarrow Ag \quad (2)$$

$$\text{Anodic } Si + 6HF \rightarrow SiF_6^{2-} + 4H^+ + 4e^- \quad (3)$$

Reaction 1 is thermodynamically favored from the calculated high standard potential up to +2.04 V. The continuous reaction produced a thick layer of Ag structures on the wafer surface (Step i, Fig. 1). The growth was ended by rinsing the wafer into water and dried in air (Step ii, Fig. 1).

The evolution of silver nanostructures was observed to depend on reaction time. At the initial stage, silver nanoparticles or nanoclusters were formed, and dendritic nanostructures with primary-order branches started to appear (Sample 1, Fig. 2A). After 30 s, obvious changes took place (Sample 2, Fig. 2B): a complex morphology with well-defined dendritic structure containing primary-, secondary-, and higher-order branches was formed. As the reaction progressed, the feather-like branches became asymmetrical, less in amount and shorter in length. And some branches were degenerated (Sample 3 and Sample 4, Fig. 2C and D). As a result, the silver structures grown in this process evolved from nanoparticles (or nanoclusters) to dendritic pattern then to fractal pattern.

To get a good understanding about the formation mechanism of the silver dendrite growth, further experiments were carried out. When another droplet (30 μL) was added, the branches appeared

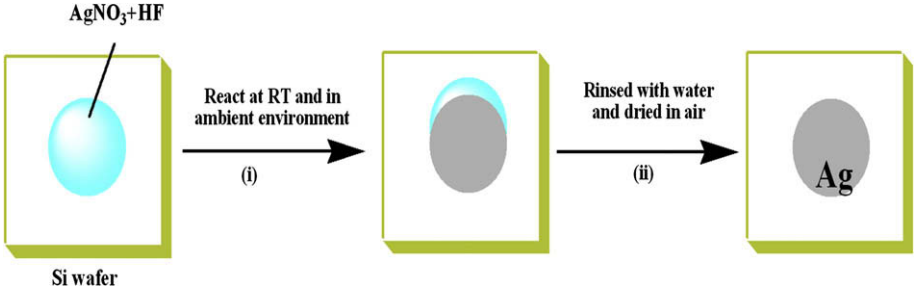

Fig. 1. Schematic illustration of the synthesizing process of silver nanostructures.

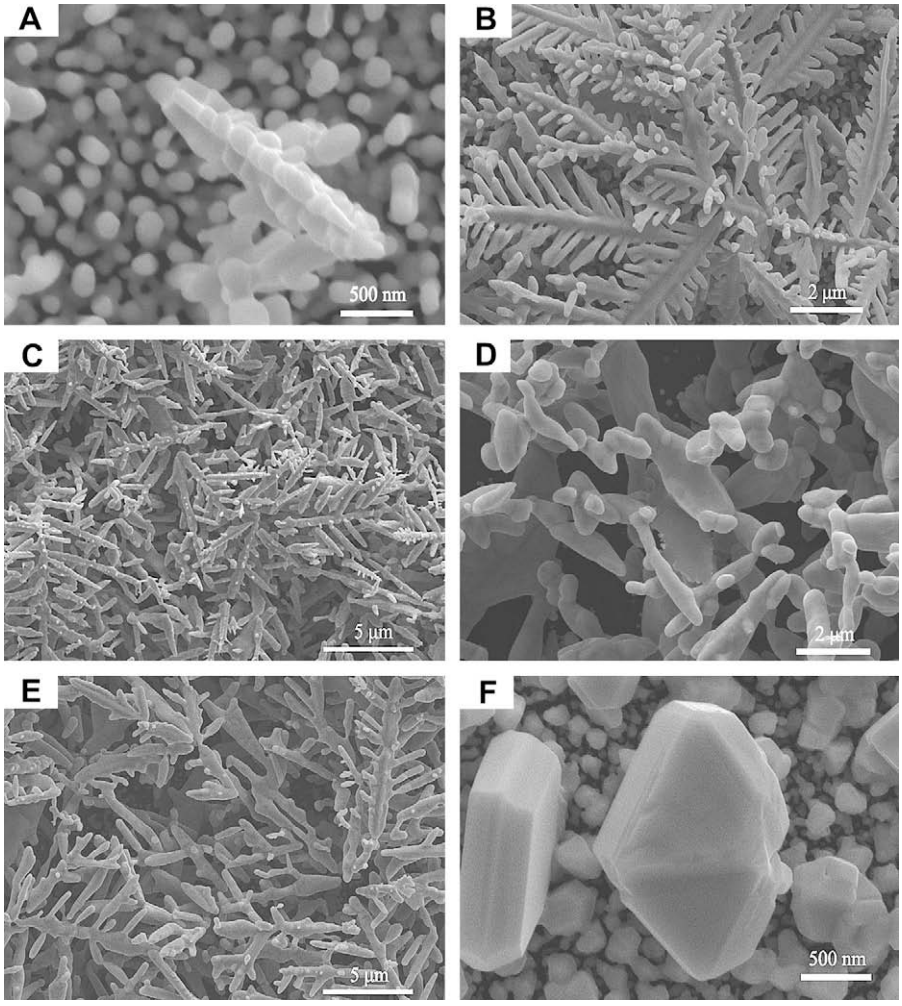

Fig. 2. SEM images of (A) Sample 1, (B) Sample 2, (C) Sample 3, (D) Sample 4, (E) Sample 5, and (F) Sample 6. Reaction conditions: room temperature, ambient environment.

again and became more and longer and symmetry (Sample 5, Fig. 2E), implying the mutual conversion between fractal and dendritic patterns at the large-scale took place. Furthermore, when substituting HF with NH_4F in the solution, only micrometer-sized silver hexagonal fractal plates were obtained, and no silver dendritic structure was observed (Sample 6, Fig. 2F).

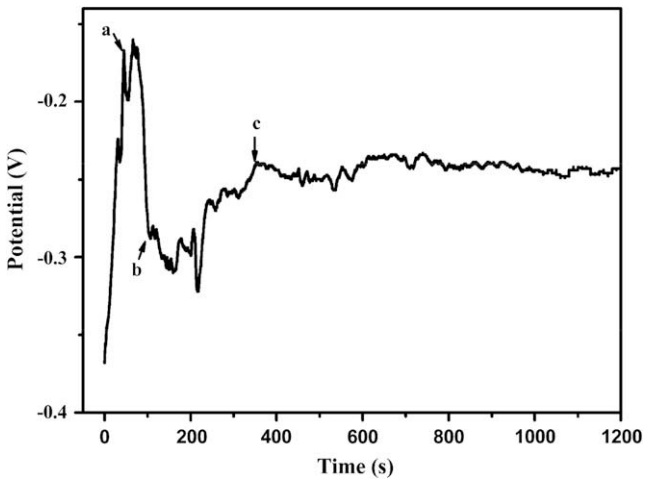

Fig. 3. Ocp-t curve. The electrolyte was 150 μL of 1.0 M HF + 0.1 M $AgNO_3$ solution. As the electrolyte was added, the scanning started immediately.

3.2. Ocp-t measurement

Ocp-t technique is a useful electrochemical technique to measure the surface site reactivity in a certain electrolyte solution, which has been used to interpret electroless metal deposition processes by our group [21,22] and others [23]. The Ocp-t curve is shown in Fig. 3. From 0 s to 45 s (at a), the open circuit potential, E_{OCP}, increased quickly from −0.368 V to −0.168 V. However, as the reaction time proceeded, from b (102 s) to c (348 s), E_{OCP} increased very slowly with small fluctuations. The potential shifted from −0.287 V to −0.238 V. And with time going on, E_{OCP} kept unchangeable.

On the basis of the mixed potential theory [24], E_{OCP} can be expressed by the following equation [23]:

$$E_{OCP} = \frac{\alpha E_1 + \beta E_2}{\alpha + \beta} + \frac{RT}{nF(\alpha + \beta)} \ln \frac{j_C}{j_A} \quad (4)$$

where E_1, E_2, α and β are, respectively, the equilibrium potentials and the transfer coefficients of the anodic and cathodic electrochemical reactions. j_A and j_C are the exchange current densities, characteristic of the rate the electron transfer proceeds on anodic and cathodic sites. In this work, the concentration of HF is ten times

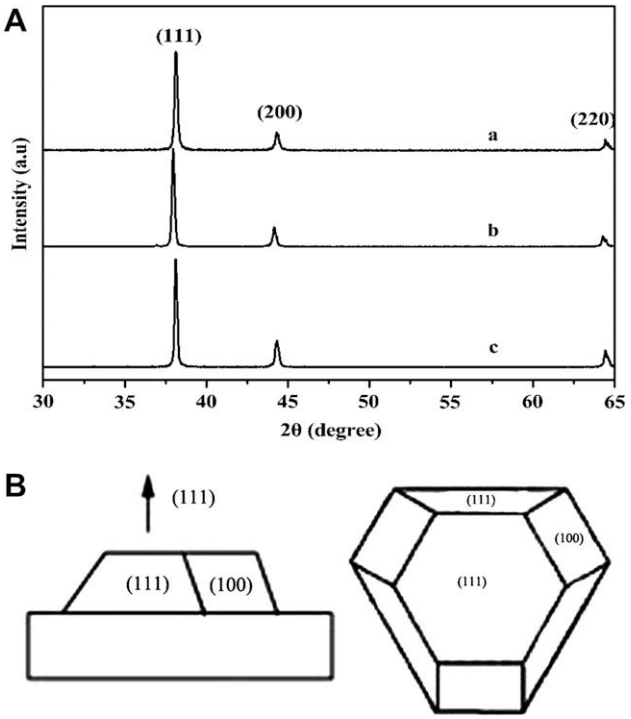

Fig. 4. (A) XRD patterns of Sample 2 (curve a), Sample 4 (curve b) and Sample 6 (curve c). (B) Profile view and top view of a truncated tetrahedral crystal (111) oriented on the substrate.

larger than that of Ag^+, so, the slope of the shift E_{OCP}, $K_{\Delta E(OCP)/t}$, can be written as:

$$K_{\Delta E(OCP)/t} = \frac{E_{OCP}(t_2) - E_{OCP}(t_1)}{t_2 - t_1} = \frac{RT}{nF(t_2 - t_1)(\alpha+\beta)} \ln\frac{j_C(t_2)}{j_C(t_1)} \quad (5)$$

where $E_{OCP}(t_1)$ and $E_{OCP}(t_2)$ stand for the values of E_{OCP} at t_1 and t_2, respectively.

Therefore, at the early reaction time, the silver deposition is under the kinetic growth process and the amount of silver deposits increased. From b to c, the slowly increased E_{OCP} with small fluctuations implies that a thermodynamic quasi-equilibrium or equilibrium condition might control the reaction. And from c then, the unchanged E_{OCP} suggests that the reaction almost ceased. The period of changed E_{OCP} was in agreement with that of SEM morphological evolution, so the evolution process of silver nanostructures was controlled by thermodynamic or kinetic factors.

3.3. XRD analysis

X-ray diffraction was performed to investigate the crystal structure. Fig. 4A displays the resulting XRD patterns of Sample 2 (curve a), Sample 4 (curve b) and Sample 6 (curve c). The peaks at $2\theta \sim 38.0°$, 44.2°, and 64.2° are assigned to the diffractions of (111), (200) and (220), respectively, indicating that the Ag deposits are in crystalline phase and the *fcc* structure (JCPDS, 4-0787). [111]/[200] and [111]/[220] ratios of intensities of diffraction lines are calculated and listed in Table 1. It is obvious that Sample 2 has the highest [111]/[200] and [111]/[220] ratios. The results reveal that the dendritic structure has a significantly higher (111) reflection intensity than the fractal structure. As drawn in Fig. 4B, for *fcc* structural metals, the flat top and bottom faces of these hexagonal plates should be bound by ⟨111⟩ plane, and the side faces of a hexagonal nanoplate must be bound by a mixture of ⟨100⟩ and ⟨111⟩ planes [25–27]. Hence, the XRD measurements confirm that dendritic nanostructures have preferentially oriented ⟨100⟩ direction.

Table 1
The ratios of intensities between different diffraction lines from XRD data.

The ratio of intensities	Sample 2	Sample 4	Sample 6
[111]/[200]	5.80	4.90	4.16
[111]/[220]	10.18	9.35	6.58

3.4. An explanation for the structural conversion

For crystals with an underlying cubic symmetry, solid–liquid interfacial energy, $\gamma(\tilde{n})$, can be expanded in the form [9]:

$$\gamma(\theta,\varphi) = \gamma_0[1 + \varepsilon_1 K_1(\theta,\varphi) + \varepsilon_2 K_2(\theta,\varphi) + \ldots] \quad (6)$$

where γ_0 is the mean value of γ, θ and φ are the special angular coordinates of the interface normal, ε_1 and ε_2 are the anisotropy parameters and K_1 and K_2 are cubic harmonics that are combinations of standard spherical harmonics $Y_{lm}(\theta,\varphi)$ with cubic symmetry [28–30]. For a wide range of *fcc* metals, and ε_2 is negative whereas ε_1 is positive. Here, a schematic diagram for the structural evolution of silver nanostructures is illustrated in Fig. 5. As $\gamma(\tilde{n})$ is positively weighted, the competition of the growth between fractal and dendritic nanostructures is under kinetic control, first cubic harmonics favors ⟨100⟩ direction and thus contributes to the dendritic growth. In contrast, as $\gamma(\tilde{n})$ is negatively weighted, thermodynamic factor dominates the reaction, second cubic harmonics favors ⟨110⟩ direction, and the transition to fractal structures is observed. And more importantly, orientation selection accompanies with fluid flow and mass transport [31,32].

In this experiment, the observed morphological evolution can be understood by the above schematic diagram. At the early stage (e.g., within 30 s), the reaction process was dominated by a non-equilibrium condition (under kinetic factor) due to a high silver ion concentration, so a dendritic morphology was formed. However, with the reaction time going on and the drop of the silver ion concentration, the reaction process was dominated by

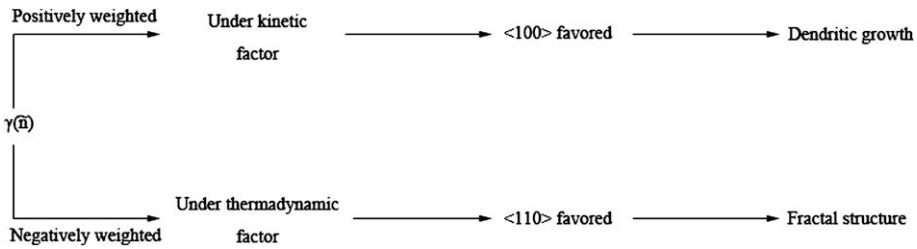

Fig. 5. A schematic diagram for the structural direction selection of silver nanostructures.

a quasi-equilibrium or equilibrium condition. The branches became less and shorter, and finally a fractal pattern was formed. As the silver ion concentration increased again, well-defined dendrites were observed again (Sample 5). That is to say, the structural conversion of between fractal and dendritic patterns structure takes place, companying with mass motion.

Well-defined silver nanodendrites were also obtained by immersing silicon substrate into the solution of NH_4F–$AgNO_3$ at 50 °C [3]. However, the structure of Sample 6 was only the hexagonal fractal plate pattern. The result demonstrates that $\gamma(\tilde{n})$ is closely related to the reaction composition and temperature.

3.5. SERS studies

The fabrication strategy of Ag nanostructures using replacement reaction has the key advantage of considerably reduced cost and free from adsorbed species, such as hydrophobic surfactants that are used in self-organizing methods [33], which are beneficial to SERS. Fig. 6(A) and (B), shows Raman spectrum of pure R6G powder and the SERS spectra of 10 μM R6G ethanol solution adsorbed on silver dendritic (Sample 2) and fractal (Sample 4) nanostructures and hexagonal fractal plate (Sample 6), respectively. Nearly no signals were observed in the spectra of pure R6G (Fig. 6A), while a number of intense peaks are seen in the spectra (Fig. 6B).

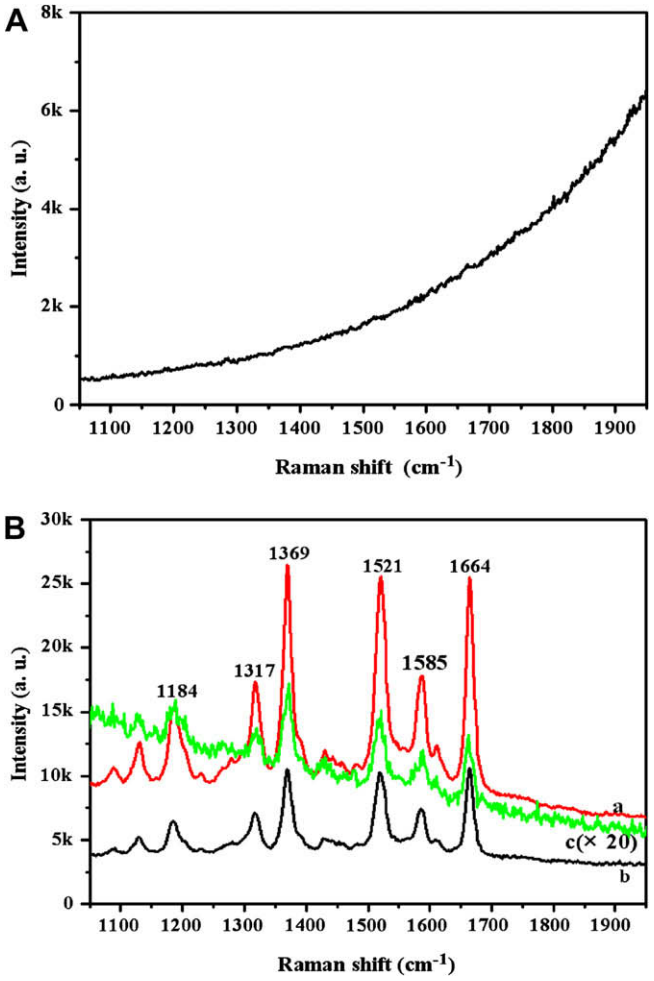

Fig. 6. (A) Raman spectrum of R6G powder. (B) The SERS spectra acquired from 10 μM R6G ethanol solution adsorbed on the surfaces of Sample 2 (a), Sample 4 (b) and Sample 6 (c). The intensity of (c) was magnified by 20-fold.

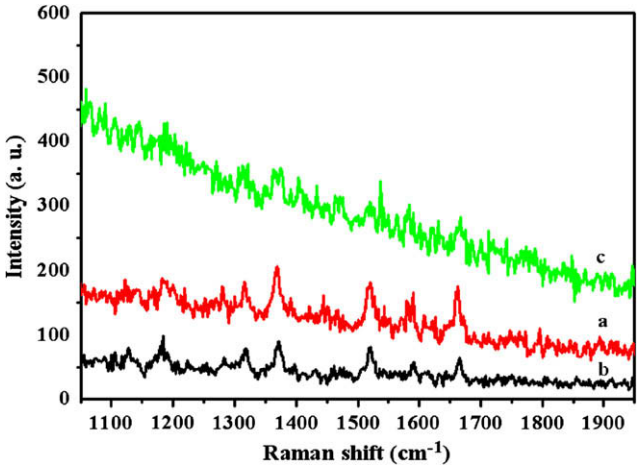

Fig. 7. The SERS spectra acquired from 1 nM R6G ethanol solution adsorbed on the surfaces of Sample 2 (a), Sample 4 (b) and Sample 6 (c).

Pronounced peaks at 1317, 1369, 1521, 1585 and 1664 cm^{-1} can be assigned to aromatic C–C stretching vibrations. The band at 1184 cm^{-1} is assigned to aromatic C–H bending [34]. On comparison of peak intensity of SERS spectra of the three silver nanostructures, it can be seen that the dendritic nanostructure (Fig. 6B(a)) had the highest enhancement factor for the probing molecules and the enhancement factor for the hexagonal fractal plate (Fig. 6B(c)) was much lower than those of the other nanostructures. The peak intensity for dendritic nanostructure is two and fifty times larger than that of the fractal nanostructure (Fig. 6B(b)) and hexagonal fractal plate, respectively. As the concentration of R6G was significantly lower (up to 1 nM), similar results were obtained, which are shown in Fig. 7. They all afford the distinct band enhancement. The present method is promising for the fabrication of stable silver nanostructures for ultrasensitive measurements.

It is well known that SERS is sensitive to the surface with metal nanoparticles. The shape and size of the metal nanoparticles strongly affect the strength of the enhancement because these factors influence the ratio of absorption to scattering events [35]. There is an ideal size for these particles – not just any small particles will have the same impact on Raman intensity – as well as an ideal size for each experiment [36]. Large particles allow the excitation of multipoles, which are nonradiative. As only the dipole transition leads to Raman scattering, the higher-order transitions will cause a decrease in overall efficiency of the enhancement. Small particles, however, will lose their electrical conductance and cannot enhance the field as well.

4. Conclusions

A simple and efficient approach was developed to fabricate hierarchical dendritic silver nanostructures, consisting of dendritic and fractal patterns, which involves replacement reaction between aqueous solution of HF-$AgNO_3$ and silicon wafers. The nanostructures evolved with time. The Ocp-t and XRD results reveal that the structure directions are determined by $\gamma(\tilde{n})$ (determined by the reaction composition and temperature), the fluid flow and mass motion, leading to the structural conversion between fractal and dendritic nanostructures. The SERS activity of the various silver nanostructures was evaluated with Rhodamine 6G (R6G) as the probe. The enhancement increases in the order of compacted hexagonal fractal plate < fractal nanostructure < dendritic nanostructure.

Acknowledgment

This work was supported by the National Science Foundation of China under Grant Nos. 20577017 and 60571045.

References

[1] A. Roucoux, J. Schulz, H. Patin, Chem. Rev. 102 (2002) 3757.
[2] Y. Sun, Y. Xia, Science 298 (2002) 2176.
[3] W. Ye, C. Shen, J. Tian, C. Wang, L. Bao, H. Gao, Electrochem. Commun. 10 (2008) 625.
[4] X. Wen, Y. Xie, M.W.C. Mak, K.Y. Cheung, X. Li, R. Renneberg, S. Yang, Langmuir 22 (2006) 4836.
[5] K. Peng, Y. Yan, S. Gao, J. Zhu, Adv. Funct. Mater. 13 (2003) 127.
[6] T. Qiu, X. Wu, Y. Mei, P. Chu, G.G. Siu, Appl. Phys. A 81 (2005) 669.
[7] T. Qiu, X. Wu, G.G. Siu, P. Chu, J. Electron. Mater. 35 (2006) 1879.
[8] S.Z. Wang, H.W. Xin, J. Phys. Chem. 104 (2000) 5681.
[9] T. Haxhimali, A. Karma, F. Gonzales, M. Rappaz, Nat. Mater. 5 (2006) 660.
[10] L. Lu, A. Kobayashi, Y. Kikkawa, K. Tawa, Y. Ozaki, J. Phys. Chem. B 110 (2006) 23234.
[11] J. Fang, H. You, C. Zhu, P. Kong, M. Shi, X. Song, B. Ding, Chem. Phys. Lett. 439 (2007) 204.
[12] J. Fang, X. Ma, H. Cai, X. Song, B. Ding, H. You, Appl. Phys. Lett. 89 (2006) 173104.
[13] K. Bromann, H. Brune, H. Roder, K. Kern, Phys. Rev. Lett. 75 (1995) 677.
[14] J.H. Kang, X.Y. Zhang, Chem. Mater. 18 (2006) 1318.
[15] F.A. Möller, O.M. Magnussen, R.J. Behm, Phys. Rev. Lett. 77 (1996) 5249.
[16] M. Fleischmann, P.J. Hendra, A.J. McQuillan, Chem. Phys. Lett. 26 (1974) 163.
[17] S. Eustis, M.A. El-Sayed, J. Appl. Phys. 100 (2006) 44324.
[18] H. Lin, J. Mock, D. Smith, T. Gao, M. Sailor, J. Phys. Chem. B 108 (2004) 11654.
[19] Y. Sun, Y. Xia, J. Am. Chem. Soc. 126 (2004) 3892.
[20] Y.Y. Song, Z.D. Gao, J.J. Kelly, X.H. Xia, Electrochem. Solid State Lett. 8 (2005) C148.
[21] H. Tong, C. Wang, Appl. Phys. A 81 (2005) 137.
[22] W. Ye, Y. Chang, C. Ma, B. Jia, G. Cao, C. Wang, Appl. Surf. Sci. 253 (2007) 3419.
[23] V. Bertagna, F. Rouelle, G. Revel, M. Chemla, J. Electrochem. Soc. 144 (1997) 4175.
[24] M. Paunovic, Plating 55 (1968) 1161.
[25] Z.L. Wang, J. Phys. Chem. B 104 (2000) 1153.
[26] Y. Xiong, J.M. McLellan, J. Chen, Y. Yin, Z. Li, Y. Xia, J. Am. Chem. Soc. 127 (2005) 17118.
[27] M. Maillard, S. Giorgio, M.P. Pileni, Adv. Mater. 14 (2002) 1084.
[28] F. Von der Lage, H.A.A. Bethe, Phys. Rev. 71 (1947) 612.
[29] J.J. Hoyt, M. Asta, A. Karma, Mater. Sci. Eng. R 41 (2003) 121.
[30] S.-K. Chan, H.-H. Reimer, M. Kahlweit, J. Cryst. Growth 32 (1976) 303.
[31] V. Fleury, J.H. Kaufman, D.B. Hibbert, Nature 367 (1994) 435.
[32] C. Sun, M. Wang, J. van Esch, G. Wildburg, W.J.P. van Enckevort, N.B. Ming, P. Bennema, R.J.M. Nolte, Phys. Lett. A 237 (1998) 247.
[33] X. Wang, H. Itoh, K. Naka, Y. Chujo, Langmuir 19 (2003) 6242.
[34] J. Zhang, X. Li, X. Sun, Y. Li, J. Phys. Chem. B 109 (2005) 12544.
[35] R. Aroca, Surface-Enhanced Vibrational Spectroscopy, UK John Wiley & Sons Ltd., 2006.
[36] L.-L.B.S.M. Mahurin, C.-D.L.S. Dai, J. Raman Spectrosc. 34 (2003) 394.